ELSEVIER

Thermochimica Acta 377 (2001) 113–124

thermochimica acta

www.elsevier.com/locate/tca

Glass transition cooperativity from heat capacity spectroscopy — temperature dependence and experimental uncertainties

H. Huth[a], M. Beiner[a,*], S. Weyer[b], M. Merzlyakov[b], C. Schick[b], E. Donth[a]

[a]*Fachbereich Physik, Universität Halle, D-06099 Halle, Germany*
[b]*Fachbereich Physik, Universität Rostock, D-18051 Rostock, Germany*

Received 15 February 2001; received in revised form 28 March 2001; accepted 30 March 2001

Abstract

The influence of experimental uncertainties of calorimetric parameters from heat capacity spectroscopy on the temperature-dependent glass transition cooperativity N_α from the fluctuation approach is studied. Glass transition parameters from 3ω method and temperature modulated DSC are compared. The influence of the stationary temperature field on the output of the 3ω method is studied. Special advantages and disadvantages of 3ω method and temperature modulated DSC for the determination of glass transition cooperativity are discussed. It is confirmed that the temperature-dependent cooperativity indicates, independent from experimental uncertainties, a cooperativity onset in the crossover region. The extrapolated onset temperature T_{on} from calorimetry is shown to be comparable with other, independently obtained crossover temperatures for polystyrene and styrene butadiene rubber (SBR 1500). © 2001 Elsevier Science B.V. All rights reserved.

Keywords: Glass transition; Heat capacity; Temperature dependence

1. Introduction

The discussion about glass transition cooperativity and the corresponding dynamic heterogeneity of glasses is a long-running issue. Glass transition research before 1980 was the domain of physicochemistry and restricted to frequencies below MHz. Molecular cooperativity was a well-defined and generally accepted concept to describe molecular movement in cold liquids [1,2]. After the development of dynamic neutron scattering in the GHz range [3,4] and a theory [5] for the dynamic glass transition at such high frequencies and for colloid glass transitions — the mode coupling theory — the glass transition terminology was dominated by physics. It is an irony of glass transition history that a real crossover in the material behavior along the trace of the dynamic glass transition was detected [6–10] for many glasses just at the borderline between the physics and physicochemistry domains in the MHz to GHz frequency range. This and other recent findings like the observation of dynamic heterogeneities in molecular dynamic simulations [11], in multi-dimensional NMR experiments [12,13] or, more phenomenologically, in experiments in confined geometries [14,15] have brought back the general interest to the glass transition cooperativity issue.

The fluctuation approach [16] developed in the late 1970s permits to calculate the cooperativity N_α, i.e. the

* Corresponding author. Tel.: +49-345-552-5350; fax: +49-345-552-7017.
E-mail address: beiner@physik.uni-halle.de (M. Beiner).

PII: S0040-6031(01)00546-9

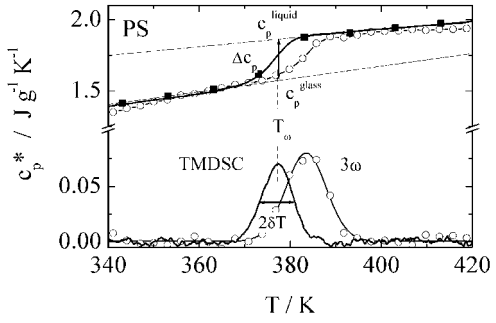

Fig. 1. Example for the determination of glass transition parameters, $T_\omega, \delta T$ and $\Delta C_p = C_p^{\text{liquid}} - C_p^{\text{glass}}$ from heat capacity spectroscopy (HCS) data. TMDSC data (bold line: period $t_p = 60$ s, $dT/dt = -0.25$ K min^{-1}, temperature amplitude $A_T = 1$K) and data from the 3ω method (◯, $f = 1.1$ Hz) for polystyrene are compared. Precise (better than ±0.5%) TMDSC data from [45] (■) are included for comparison.

number of particles (monomeric units) in a cooperatively rearranging region (CRR), and the characteristic length of glass transition ξ_α (CRR size) from calorimetric data according to

$$N_\alpha = \frac{\xi_\alpha^3 \rho N_A}{M_0} = \frac{RT^2\Delta(1/C_V)}{M_0\delta T^2} \approx \frac{RT^2\Delta(1/C_p)}{M_0\delta T^2} \qquad (1)$$

with $\Delta(1/C_p) = 1/C_p^{\text{glass}} - 1/C_p^{\text{liquid}}$ being a measure of the calorimetric intensity of dynamic glass transition, δT being the temperature fluctuation as obtained from the width of the dynamic glass transition (see below, Fig. 1), T_ω the dynamic glass transition temperature for the frequency ω, R the gas constant, N_A the Avogadro number, and M_0 the molecular weight of the relevant particle. Further details, the thermodynamic background, and theoretical uncertainties of Eq. (1) are discussed in detail in [15,17,18].

Heat capacity spectroscopy HCS methods like 3ω method [19–21] and temperature modulated DSC (TMDSC) [22–24] developed and established in the last two decades allow to study the temperature dependence of cooperativity along the trace of dynamic glass transition in an Arrhenius plot [25,26]. All calorimetric parameters in Eq. (1) can be determined by HCS for different frequencies ω or corresponding temperatures (T_ω). Thus, temperature-dependent cooperativities $N_\alpha(T_\omega) \equiv N_\alpha(T)$ are available in a relatively wide range.

New stimulation for such studies came from the experimental finding that the cooperativity has an onset in the crossover region, where many other properties of the dynamic glass transition are also changing. For poly(*n*-hexyl methacrylate) and some related materials this onset was directly observed [27] inside the frequency window the 3ω method as saddle-like peculiarity in the imaginary part of $\rho\kappa C_p''(\omega, T)$ between α-relaxation below the crossover and high temperature process *a* above the crossover.

It is now established that the crossover region is important for an understanding of the dynamic glass transition [10,28–30]. Crossover temperatures obtained from independent methods are often in good agreement [31]: relaxation times of dynamic glass transition (*a* and α processes) and Johari Goldstein mode (β process) approach one another (T_β) [8], the temperature dependence of the viscosity changes from one to another WLF parameter set (T_B) [7], and the translational diffusion enhances from rotational diffusion (T_{r-t}) [10] at comparable temperatures. Temperature-dependent cooperativities from HCS experiments indicate that this consistency is related to an onset of molecular cooperativity [25,31].

Unfortunately, there are only a few glass formers with a crossover frequency in the mHz to kHz frequency window accessible for HCS methods. It was also attempted [25,26] to extrapolate the temperature-dependent cooperativity into the crossover region using the following formula from a fluctuation approach

$$\text{Fluctuation approach}: \quad N_\alpha^{1/2}(T) = A\left(\frac{T_{on} - T}{T - T_0}\right) \qquad (2)$$

with T_0 being the Vogel temperature as obtained from a fit to the α-trace below the crossover region by a WLF equation, T_{on} the onset temperature where the extrapolated cooperativity approaches formally zero, and *A* a material-specific parameter of order 5–10. Eq. (2) usually approximates the temperature dependence of cooperativity adequately. Studies on several substances indicate that the extrapolated cooperativity approaches zero in the same temperature range where the other peculiarities of the dynamic glass transition can be observed from independent methods, i.e. an onset of the intermolecular cooperativity in the crossover region is indicated.

It is well known, however, that there are large uncertainties of calorimetric parameters for the

calculation of glass transition cooperativity [32]. The uncertainty for the N_α values calculated from temperature modulated DSC data near T_g was estimated recently [17] to be a factor of 2 (50–200%). This requires to study the influence of experimental uncertainties on the cooperativity, on its temperature dependence and finally on the extrapolated cooperativity onset temperatures T_{on} in detail.

Temperature-dependent cooperativities for two standard glass formers, polystyrene and styrene butadiene rubber, will be discussed in this paper. Especially, it will be shown by a combination of HCS data from 3ω method and TMDSC and by a study of the influence of stationary temperature fields on the output of the 3ω method that random and systematic uncertainties of calorimetric data from the 3ω method do not change the main conclusion of above discussed studies: a cooperativity onset in the crossover region. A detailed comparison of advantages and disadvantages of both methods of HCS for this purpose is part of the discussion.

2. Experimental

2.1. Samples

Experiments are performed on three commercial samples: a commercial polystyrene (PS 168N) from BASF AG, a non-vulcanized styrene butadiene rubber containing 23W% styrene (SBR 1500) provided by Dr. G. Heinrich (Continental AG, Hannover), and the noncross-linked epoxy resin diglycidyl ether of bisphenol A (DGEBA, trade name: EPON828) provided by Shell AG, Germany. Density at room temperature ρ, DSC glass temperature T_g, molecular weight of monomer or molecule M_0, and the average molecular weight $\overline{M}_w$ for the polymers are given in Table 1. Experimental (see Section 3.1) and literature data for the product of density and heat conductivity $\rho\kappa$ are added. The DSC glass temperatures T_g are obtained [17] from conventional DSC scans with a heating rate of $\dot{T} = +10\ \mathrm{K\ min^{-1}}$ by an equal-area construction.

2.2. Setups

2.2.1. 3ω method

The used 3ω method setup enables isothermal effusivity, $\rho\kappa C_p^* = \rho\kappa C_p' - \mathrm{i}\rho\kappa C_p''$, measurements in the frequency range from 0.02 Hz to 4 kHz. The accessible temperature range is -150 to 250°C using different thermostats. The signal registration is done by a combination of a low noise differential amplifier with a sampling oscilloscope or a fast 12-bit A/D converter. Nickel heaters of about 60 nm thickness on poly(ether ether ketone) (PEEK) substrates are used. At least two runs with samples on nickel heaters of different size, about 10 mm × 5 mm for low frequency (0.02–20 Hz) measurements and 1.5 mm × 6 mm for the higher frequencies (2 Hz to 4 kHz), are combined. Details of the experimental setup and the external data evaluation procedure are described elsewhere [33].

2.2.2. Temperature modulated DSC (TMDSC)

The technique, described for the first time in 1971 by Gobrecht et al. [22], and the necessary data treatments are described elsewhere [22,23,34–36]. The frequency range accessible with commercial TMDSC apparatuses is very limited. Often it is less than two orders of magnitude and the high frequency limit is below 0.1 Hz. To enlarge the frequency range for TMDSC measurements DSCs with different time constants have to be combined. For this study a Perkin-Elmer Instruments Pyris 1 DSC and a Setaram

Table 1
Characteristic properties of the samples

Sample	T_g (K)	M_0 (g mol^{-1})	ρ (g cm^{-3})	$\overline{M}_w$ (kg mol^{-1})	$\rho\kappa$ (kg W m^{-4} K^{-1})	
					3ω method	Literature
PS168N	373	104	1.04	270	112, 142, 121[a]	134 [60]
SBR 1500	215	61	0.9	≈500	147, 141, 136[a]	177–233 [60]
DGEBA	254	380	1.16	–	185	170 [61]

[a] The values are obtained from three different runs by the 3ω method (see text).

DSC 121 were used [37]. The resulting frequency range was 10^{-4} to 0.1 Hz. For the comparison of various experimental datasets, a careful temperature calibration of all instruments is necessary. The DSCs are calibrated at zero heating rate according to the GEFTA recommendation [38]. The calibration was checked in TMDSC mode with the smectic A to nematic transition of the liquid crystal 8OCB [39,40]. To avoid falsification of the dynamic heat capacity by partial vitrification [41] a constant ratio between underlying cooling rate and frequency of temperature oscillation of 15 K min^{-1} Hz^{-1} was used for all measurements.

2.3. Simulations

The stationary temperature field near the heater in our 3ω method setup was studied by finite element method (FEM) simulations. The Fluid Dynamics Analysis Package (FIDAP) by FLUENT, Inc. was used. Numerical simulations were performed for a PEEK block of 20 mm × 20 mm × 5 mm and a nickel heater of 10 mm × 5 mm with a thickness of 50 nm on top. The mesh consists of about 22 000 elements for PEEK and 600 elements for nickel. Boundary conditions are constant temperature at the bottom of the PEEK block and an adiabatic situation on all other boundaries. The heat production for all nickel elements was 28×10^9 W m^{-3} consistent with a heater power of 70 mW.

3. Results and discussion

Main interest of this study is the influence of experimental uncertainties on the absolute values of temperature-dependent glass transition cooperativity from Eq. (1). In particular, the consequences of these uncertainties for special extrapolations (Eq. (2)) and for the relation between cooperativity onset temperature T_{on} and crossover temperatures from independent methods will be considered.

There are three calorimetric parameters which have to be determined in order to calculate the temperature-dependent cooperativity $N_\alpha(T)$ from Eq. (1): the calorimetric α relaxation strength $\Delta(1/C_p)$, the dynamic glass transition temperature T_ω, and the temperature width of the α peak for a given frequency, δT. Two of these calorimetric parameters $(T_\omega, \delta T)$ can be taken from a fit to the imaginary part of the 3ω or TMDSC output for a given frequency, $\rho\kappa C_p''(T)$ or $C_p''(T)$, with a Gaussian function (Fig. 1). It is confirmed that a Gaussian function reasonably approximates the peak of the dynamic glass transition in $C_p''(T)$ isochrones as long as no vitrification occurs and the sample is in the liquid state [41]. Keeping this condition, often difficult in TMDSC measurements, there are only deviations on the peak wings near the base-line which do not affect the determination of peak width (δT) and peak position (T_ω). For the TMDSC measurements the fit was restricted to temperatures above the beginning of vitrification on cooling, for details see [41]. The third parameter $(\Delta(1/C_p) = 1/C_p^{\text{glass}} - 1/C_p^{\text{liquid}} \approx 4\Delta C_p/(C_p^{\text{glass}} + C_p^{\text{liquid}})^2)$ can be obtained from a tangent construction to the real parts, $\rho\kappa C_p'$ or C_p', respectively (Fig. 1).

A combination of different methods of HCS is used to estimate experimental uncertainties of the cooperativity values calculated from calorimetric data. We will present (Section 3.1) a detailed comparison of results from the 3ω method and temperature modulated DSC for polystyrene (PS 168N). Independently determined calorimetric parameters for the dynamic glass transition are compared and the resulting uncertainty of the temperature-dependent cooperativities (Eq. (1)) is estimated. In Section 3.2 the systematic influence of the stationary temperature field on the output of the 3ω method and the glass transition parameters is discussed. The wide accessible frequency temperature range is used (Section 3.3) to check the approximation of temperature-dependent cooperativities by Eq. (2). The influence of experimental uncertainties on the extrapolated cooperativity onset temperature T_{on} is discussed.

3.1. Comparison of cooperativities from 3ω method and temperature modulated DSC

Calorimetric parameters for PS 168N obtained from three independent 3ω runs on different heaters in the frequency range from 0.02 Hz to 2 kHz (cf. Fig. 2) and several TMDSC measurements in the range from 10^{-4} to 0.1 Hz are shown in Fig. 3. The open symbols are obtained by an independent analysis of all isofrequency curves of different runs by the 3ω method. The parameters T_ω and δT from 3ω method and

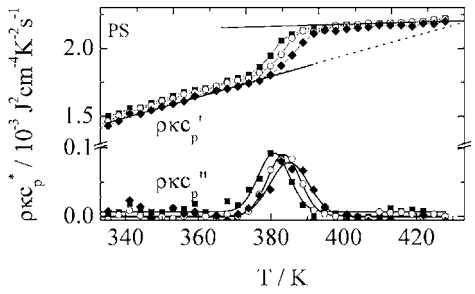

Fig. 2. Real and imaginary parts of dynamic effusivity $\rho\kappa C_p^*$ for polystyrene (PS168N). Isochrons at 0.35 Hz (■), 1.1 Hz (◯), and 3.5 Hz (◆) from the 3ω method are shown. The drawn tangents indicate $\Delta C_p \rightarrow 0$ at 433 K.

TMDSC are in good agreement. There is, however, a certain discrepancy between the temperature-dependent ΔC_p values from both methods of HCS and a mismatch of the uncorrected ΔC_p values from two 3ω runs. In the following we will discuss in some detail the uncertainties of the calorimetric parameters from the different methods considering especially the effects important for the calculation of cooperativity.

3.1.1. 3ω method

There are two reasons that make it attractive to investigate the glass transition cooperativity and its temperature dependence by the 3ω method: (i) Calorimetric data for the dynamic glass transition can be obtained in a wide frequency range (0.02 Hz to 4 kHz) on one and the same sample. (ii) The dynamic glass transition is detected for the available frequencies in thermodynamic equilibrium because the test frequencies are high enough compared to equilibrating times of about 30 min prior to the isothermal frequency sweeps. Non-equilibrium situations are only expected in the glassy state below the conventional DSC glass temperature T_g.

The disadvantages of the 3ω method are: (i) the large uncertainty (about $\pm 40\%$) of absolute $\rho\kappa C_p^*$ values due to uncertainties of the effective heater size, the reproducibility of the baseline for the substrate, and the risk of time-dependent changes of the heater resistance. (ii) The 3ω method measures primary effusivities $\rho\kappa C_p^*$. To get glass transition parameters, especially ΔC_p, from effusivity data one has to correct the 3ω output for $\rho\kappa$. Unfortunately, qualified heat conductivity data in a large temperature range are

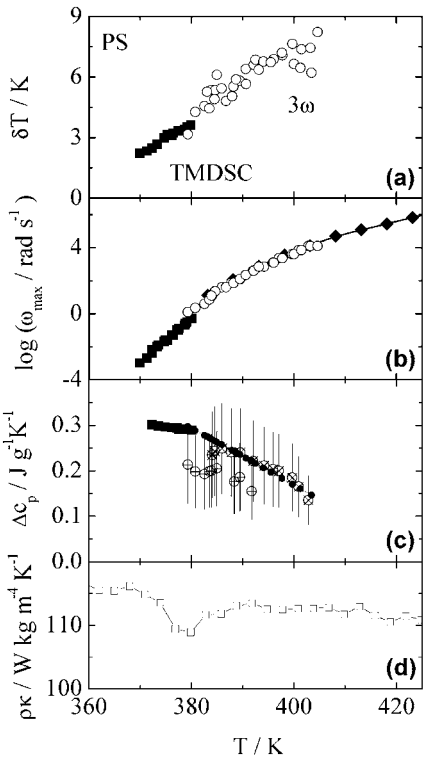

Fig. 3. Peak width δT (a), logarithm of frequency $\log \omega_{max}$ (b), and ΔC_p (c) as function of temperature T_ω for polystyrene (PS168N) from TMDSC (■) and 3ω method (◯). Dielectric data (◆) are added in part (b). The ΔC_p values from the 3ω method in (c) result from a tangent construction for each isochron of the two different runs (⊕, ⊗) corrected by a fixed factor $\rho\kappa = 128$ kg W m^{-4} K^{-1}. The error bars indicate an uncertainty of $\pm 40\%$. The values from the common tangent construction with individual adjustment of both runs to TMDSC data (•) are also shown in part (c). The $\rho\kappa$(T) curve (d) is obtained by dividing a $\rho\kappa C_p'$ ($f = 0.2$ Hz) curve from the 3ω method by a C_p' curve ($t_p = 60$ s) from TMDSC. The minimum near 380 K is due to the frequency shift between both curves.

usually not available. Frequency-dependent heat conductivity measurements are possible (e.g. by the 3ω method [42,43]) but very time consuming. The common result of frequency-dependent $\rho\kappa$ measurements on selected glasses is that the heat conductivity at the glass transition does not depend on frequency [42–44]. Thus, a fixed factor $\rho\kappa$ correction is commonly used.

In our case, the temperature dependence of heat conductivity above and slightly below the DSC glass transition temperature was estimated by the ratio between the output from 3ω method and TMDSC

$\rho\kappa C'_p/C'_p$ (Fig. 3d). The $\rho\kappa$ value of our PS 168N sample does not dramatically depend on temperature in the range from 370 to 420 K where the dynamic glass transition for our test frequencies occurs. It seems adequate to use a frequency- and temperature-independent $\rho\kappa = \text{const.}$ mean values determined from the data of each 3ω run for the correction. The obtained $\rho\kappa$ values are in agreement with literature values for polystyrene (Table 1). The different $\rho\kappa$ mean values obtained for different 3ω runs reflect the absolute uncertainty of 3ω data ($\pm 40\%$, see above).

The consequence of this uncertainty is the remarkable difference between the absolute ΔC_p values from different runs of the 3ω method if they are corrected with a fixed factor from the literature for $\rho\kappa$ ($\oplus\otimes$ in Fig. 3c). The uncertainty decreases if a specific $\rho\kappa$ mean value (Table 1) is used for each run and common tangents for all frequencies are considered ($\bullet$ in Fig. 3c). The relative uncertainty comparing the ΔC_p values for different frequencies of one run (about $\pm 10\%$) is always smaller than the absolute one and results. It results mainly from the uncertainty of the tangent construction in Fig. 1: heater, baseline or $\rho\kappa(T)$ effects are less important at this point. We notice that the temperature dependencies of ΔC_p from the 3ω method and from TMDSC are different (Fig. 3c). This is a consequence of differences between both methods in the slope of the $C'_p(T)$ tangents. The temperature where a *linear* extrapolation $\Delta C_p(T) \rightarrow 0$ from TMDSC approaches zero is often significantly higher than the corresponding temperature from the 3ω method. The reason for this discrepancy is not completely clear so far. It possibly reflects a non-linear temperature dependence of $\Delta C_p(T)$, the temperature dependence of $\rho\kappa$, or differences in the non-equilibrium state below the dynamic glass transition measured by the two methods. Precise heat conductivity measurements in a wide temperature range could contribute to a clarification of this problem. The temperature-dependent cooperativity $N_\alpha(T)$ is less affected by the tangent problem because ΔC_p is relatively locally defined for each isotherm. Moreover, ΔC_p is only one of the calorimetric parameters in Eq. (1).

The scatter in δT values from different 3ω runs is relatively small ($< \pm 0.5$ K) and mainly a consequence of uncertainties of the Gauss fit due to the scatter in the $\rho\kappa C''_p$ data. The influence of $\rho\kappa(T)$ on the determination of peak width δT is expected to be small because the relevant temperature range is small ($\delta T \approx 10$ K). The $\rho\kappa = \text{const.}$ approximation is applicable in this temperature interval, because $\rho\kappa$ changes are negligible. The contributions from a systematic error due to the stationary temperature field around the heater are discussed in Section 3.2.

The uncertainty of the dynamic glass transition temperature T_ω is about ± 1 K and results from fit uncertainties and from problems with the heater temperature calibration. Systematic contributions to the absolute T_ω uncertainty due to the stationary temperature gradient in our samples are included. The temperature can at best be measured at the surface of the heater. Parts of the sample and the substrate away from the heater surface with a lower temperature, however, also contribute to the signal. This is an intrinsic problem of the conventional 3ω method that could only be solved by special setups, e.g. by using Peltier elements instead of a simple heater [45]. A related problem is that there are only complicated and not extremely precise methods to calibrate the absolute temperature scale of a 3ω method setup [40,46]. The relative T_ω uncertainty comparing the dynamic glass temperatures for different frequencies from one run is smaller (about ± 0.5 K) because the temperature differences are not significantly affected by different gradients or by uncertainties of the absolute temperature scale.

3.1.2. Temperature modulated DSC

Main advantages of TMDSC measurements for the determination of cooperativity are: (i) the absolute heat capacity values C'_p are more precise. At least for long periods or low frequencies an absolute precision of the heat capacity better than $\pm 0.5\%$ can be reached [47]. This is much better than for the 3ω method. (ii) TMDSC measures directly C^*_p, i.e. it has no problems with $\rho\kappa$ apart from the high frequency limit [48]. (iii) The high sensitivity (precision) of up to date TMDSC equipment allows an extension of the available frequency range for more than two orders of magnitude towards lower frequencies. (iv) Some other specific 3ω uncertainties are also absent, e.g. TMDSC has no problem with stationary temperature fields and precise temperature calibration procedures are applicable [38–40].

However, TMDSC has also specific disadvantages: (i) the frequency range of TMDSC instruments is limited. At short periods or high frequencies the uncertainty of commercial TMDSC setups increases significantly. Heat transfer problems occur which must be corrected by baseline correction methods for the imaginary part C_p''. The C_p' data must partly be adjusted to low frequency measurements. (ii) TMDSC results are more affected by non-equilibrium problems because the interference of the dynamic glass transition with vitrification of the sample [41] is unavoidable at low frequencies. (iii) A TMDSC run gives usually data for only one frequency. This is a disadvantage considering studies of the temperature dependence of glass transition cooperativity because thermal history and sample preparation must be identical for the different runs. New multi-frequency [49] methods may help at this point.

Typical uncertainties for the glass transition parameters from 3ω method and TMDSC are summarized in Table 2. The resulting uncertainty of the cooperativity $N_\alpha(T)$ is also estimated. The TMDSC aspects are also discussed in [17].

We conclude from this section that temperature-dependent cooperativities $N_\alpha(T)$ can be adequately determined by a combination of highly precise TMDSC data at low frequencies and 3ω method data at higher frequencies. Data from the 3ω method are useful to study the temperature dependence of cooperativity but the discussion of absolute N_α values needs an adjustment to more precise methods concerning absolute C_p values, e.g. from TMDSC. The discussed combination of both HCS methods allows to study $N_\alpha(T)$ in a wide frequency temperature range with acceptable uncertainties.

Table 2
Typical uncertainties of glass transition parameters and cooperativity from 3ω method and TMDSC[a]

	3ω method	TMDSC
ΔC_p	±40% (±10%)	±2%
δT	±0.5 K (±0.5 K)	±0.5 K
T_ω	±1 K (±0.5 K)	±0.5 K
N_α	50–200%[b] (75–125%)[b]	75–125%[b]

[a] Relative uncertainties for the parameters from different isochrons of a single run of the 3ω method are given in parentheses.

[b] These values do not include the uncertainty of the $\Delta(1/C_V) \approx \Delta(1/C_p)$ approximation in Eq. (1) of about ±30% (see [15]).

3.2. Influence of the stationary temperature field on the output of the 3ω method

The output of the 3ω method is systematically influenced by the stationary temperature field at the heater surface and in the surrounding [50]. The theoretical model [19] for the determination of calorimetric data from the 3ω method neglects this problem. It describes the situation with a periodic temperature perturbation under otherwise isothermal conditions. The setups for the 3ω method used so far do not work under such ideal conditions. The temperature perturbation is produced by an electric heater and is intrinsically connected with the existence of stationary gradients at the heater surface as well as in substrate and sample. Effects of the stationary temperature field are especially relevant for small heaters and large heating power necessary for higher frequencies because of the specific frequency dependence of the 3ω signal ($U_{3\omega} \sim \omega^{-1/2}$).

The typical shape of the stationary temperature field in a system with a 60 nm nickel heater on a PEEK substrate is visualized in a infrared picture (Fig. 4a). There are significant temperature gradients on the surface of the nickel heater: the temperature at the center of the heater is about 5 K higher than that at the borderline of the heater. Note, that the gray level change at the borderline of the heater, indicating fictively a temperature step, is due to a difference of the emission coefficient between Nickel and PEEK substrate. The scale shown in Fig. 4a is corrected for PEEK, i.e. is only correct for the substrate.

The stationary temperature field simulated by a FEM using the commercial FIDAP program package is shown in Fig. 4b. The parameters and the simulated temperature field are comparable to the experimental situation (Fig. 4a). A histogram for the temperature distribution of the heater elements is presented in Fig. 4c. Qualitatively, the simulated temperature distribution is similar to the experimental situation. The smaller width of the experimental distribution may be due to special properties of our heaters as for example a possible thickness profile or the surface roughness of the used substrates. The mean heater temperature $\overline{T}$ used as measurement temperature is calculated

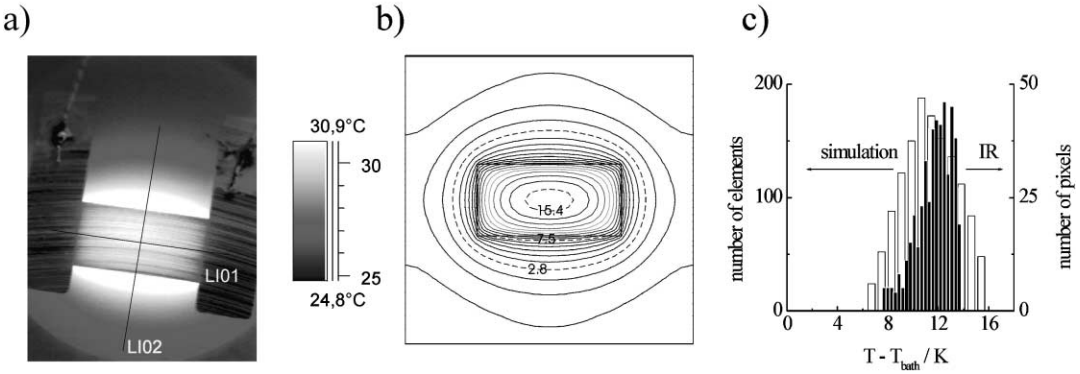

Fig. 4. Temperature field at the surface of the substrate with heater taken from (a) an infrared camera picture and (b) a FEM simulation. (c) Histogram for the temperature distributions at the heater surface from IR (right axis) and simulation (left axis). The infrared picture has 470 pixels for the nickel heater. The simulation uses 300 elements on the surface of the heater. The heater size is 5 mm × 10 mm. The temperature obtained by the infrared camera is corrected for PEEK. Emission coefficient and temperature scale for Nickel are slightly different from those for PEEK.

from the heater resistance and reflects therefore only an arithmetic average of the temperature distribution at the surface of the heater (Fig. 4c).

A comparison of data for the dynamic glass transition in styrene butadiene rubber (SBR1500) measured with different heating power (and temperature amplitude) (Fig. 5) shows that the main consequence of the stationary temperature field on the output of the 3ω method is a broadening of the dynamic glass transition, i.e. a systematically enlarged peak width δT. The fictive increase of the peak width δT due to the temperature field is about 1 K at the highest heating power under consideration. The curves in Fig. 5c are calculated as the sum

$$c_p''(\omega, T) = \frac{1}{N}\sum_{i=1}^{N} c_{p\,\max}'' \exp\left\{-\frac{(T_i - T_\omega)^2}{2\delta T^2}\right\} \qquad (3)$$

considering that the measured signal for the dynamic glass transition is a superposition of contributions from $N \approx 470$ heater elements with an individual temperature T_i. Gauss-like contributions from the different heater elements are assumed. The temperature distribution was taken from infrared experiments

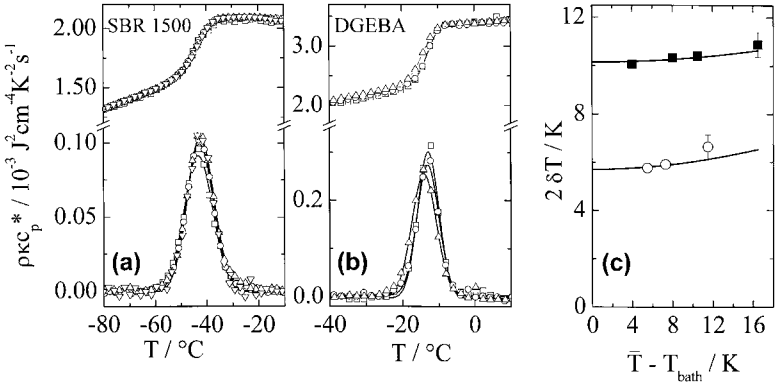

Fig. 5. Variation of 3ω method output $\rho\kappa C_p''$ with heating power for (a) SBR 1500 at 20 Hz ((□) 100 mW, (◯) 70 mW, (△) 53 mW, (▽) 27 mW) and (b) DGEBA at 0.62 Hz ((△) 128 mW, (◯) 83 mW, (□) 64 mW). (c) Peak width $2\delta T$ obtained from data in (a) and (b) as function of $\overline{T} - T_{\text{bath}}$. The lines are simulations according to Eq. (3) using the experimentally detected temperature distribution (Fig. 4).

(Fig. 4a). This simulation reasonably approximates the experimental data. From this observation and the agreement between 3ω method and TMDSC results for δT (see Fig. 3) it can be concluded that the main effect of the temperature field comes from the temperature distribution in the heater plane. The effect of temperature gradients normal to the heater surface seems to be smaller. Note, that the effect of the temperature field on δT is especially relevant for glasses with a narrow dynamic glass transition and large cooperativity like the epoxy resin diglycidyl ether of bisphenol A (Fig. 5c). Measurements and simulations show that the systematic error of the temperature width $\Delta(\delta T)$ is practically frequency-independent and independent of the sample-specific peak width δT. It depends mainly on the stationary temperature field. The influence of the stationary temperature field on the other glass transition parameters, $\Delta(1/C_p)$ and T_ω, seems to be negligible (Fig. 5a).

Summarizing this section we conclude that there is a relevant and systematic influence of the stationary temperature field on the peak width δT of the dynamic glass transition measured by conventional 3ω setups with higher heating power. The effect on δT is mainly due to the temperature distribution on the heater surface, is frequency-independent, and can be estimated by Eq. (3). The effect on the other glass transition parameters, $\Delta(1/C_p)$ and T_ω, is small.

3.3. Temperature dependence of cooperativity — crossover region of dynamic glass transition

We will discuss the uncertainty of temperature-dependent cooperativities $N_\alpha(T)$, the significance of fits to temperature-dependent cooperativity data, and the uncertainty of extrapolations made to estimate the cooperativity onset temperature T_{on}. The latter will be compared with $\alpha\beta$ splitting temperatures T_β from independent measurements.

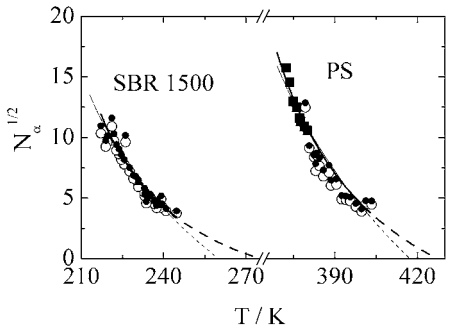

Fig. 6. Uncorrected (◯) and corrected (●) values for the cooperativity of SBR 1500 and PS168N. The cooperativities from TMDSC for PS168N (■) are added. The thick lines are fits to the corrected data from 3ω method including the TMDSC data for PS168N by the fluctuation approach (Eq. (2)). The thin lines are for the S_c approach (Eq. (4)).

Temperature-dependent cooperativities for PS 168N and SBR1500 were calculated from the original calorimetric data and from the temperature-field corrected data (Fig. 6). In general, a dramatic nonlinear decrease of cooperativity with increasing temperature is observed. The discrepancy between original and corrected $N_\alpha^{1/2}$ values, however, is comparatively small. We observe a small shift of the complete dataset to higher values. The curve shape is not significantly affected. All datasets can adequately be approximated by Eq. (2) and there is no significant difference between the fit parameters A and T_{on} for the uncorrected and corrected data (Table 3). For PS 168N cooperativities from TMDSC

Table 3
Cooperativity parameters, Vogel temperatures T_0, and $\alpha\beta$ splitting temperature T_β for PS 168N and SBR 1500

Sample		Fl approach		S_c approach T_{on} (K)	T_β (K)	T_0 (K)
		A	T_{on} (K)			
PS	3ω (uncorrected)	11.0	427	419	425 [62]	330
	3ω (corrected)	10.9	429	421		
	3ω and TMDSC	11.4	427	417		
SBR 1500	3ω (uncorrected)	6.2	277	262	300–330	184
	3ω (corrected)	6.8	275	260		

are added (Fig. 6). The cooperativities from TMDSC and 3ω method are comparable in the range where the measurement frequencies overlap. The combination of both methods leads to a extension of the accessible temperature range. The resulting fit parameter change is moderate (Table 3). Especially, the cooperativity onset temperature T_{on} is only slightly affected.

The extrapolated cooperativity for polystyrene goes to zero in the same temperature range where the relaxation times of dynamic glass transition (α) and Johari Goldstein mode (β) approach (Fig. 7). The degree of coincidence of cooperativity onset temperature T_{on} with T_β is shown for PS and SBR1500 in Table 3. This supports the recent observation that for many glasses the cooperativity onset temperature T_{on} is in agreement with crossover temperatures from the other methods ($T_\beta, T_B, T_{r-t}, T_c$) [26,31].

Alternative assumptions about the temperature dependence of cooperativity do not significantly change the T_{on} value [26]: using the predictions of configuration entropy (S_c) concepts [2,51–53] ($N_\alpha \sim (T - T_0)^{-1}$ near the Vogel temperature T_0), instead of those from the fluctuation approach ($N_\alpha \sim (T - T_0)^{-2}$ near T_0), i.e. the equation

$$S_c \text{ approach}: \quad N_\alpha^{1/2}(T) = A\left(\frac{1-x}{\sqrt{x}}\right), \qquad x = \frac{T - T_0}{T_{on} - T_0} \tag{4}$$

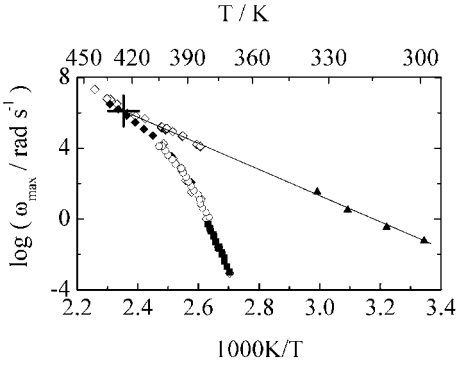

Fig. 7. Arrhenius plot for polystyrene from different calorimetric methods (TMDSC (■), 3ω method (◯)), dielectric spectroscopy (◆), NMR [62] (◇) and mechanical measurements [63] (▲). The line is a fit to the data for the β process. The cross indicates the crossover temperature T_β.

instead of Eq. (2), similar cooperativity onset temperatures (Table 2) were obtained. A final decision between both, fluctuation variant (Eq. (2)) and configuration entropy concept (Eq. (4)), is not possible (cf. Fig. 6) with the present uncertainties of calorimetric data. Although the stronger temperature dependence at low temperature favors the fluctuation variant, the temperature dependence alone cannot decide this issue [26].

Independent experiments, however, indicate that the fluctuation approach gives more realistic absolute values for cooperativity N_α and CRR size ξ_α. An analysis of calorimetric measurements [15] in confined geometries (2.5–7.5 nm) shows that the fluctuation approach gives CRR sizes in agreement with the confinement, whereas an equation based on the Gibbs distribution [54–56] gives unrealistically large CRR sizes. The temperature fluctuations as described by the von Laue [57] approach to thermodynamics which were used by the fluctuation approach to derive Eq. (1) are important [15,58] to understand the cooperative motions of the dynamic glass transition below the crossover region. The established Gibbs distribution considering only energy fluctuations is partly unable to explain these findings. Additional support for this interpretation comes from C_p measurements [59] at low temperature around 1 K for the poly(*n*-alkyl methacrylate) series. The results indicate a breakdown of the tunnel density when the cooperativity $N_\alpha(T_g)$ from the fluctuation approach based on von Laue thermodynamics becomes smaller than about 15 particles, i.e. the number of next neighbors. Using the Gibbs approach to thermodynamics, the breakdown had to be explained by a cooperativity of order of 500 monomeric units, much too large to expect structural reasons for the tunnel density breakdown. The consequence is that thermodynamics is more than a consequence of the Gibbs distribution [15].

The conclusion of this section is that temperature-dependent cooperativities for PS and SBR 1500 indicate, independent of the uncertainties of calorimetric glass-transition parameters, a cooperativity onset in the crossover region near T_β. The cooperativity onset in $N_\alpha(T)$ data from the fluctuation approach based on von Laue thermodynamics is in agreement with peculiarities in the crossover region of the dynamic glass transition obtained independently by other experimental methods.

4. Summary

A combination of data for the dynamic glass transition from 3ω method and temperature modulated DSC allows to calculate temperature-dependent cooperativities $N_\alpha(T)$ in a reasonable broad temperature range with acceptable uncertainties. The cooperativity values in the overlap range of both calorimetric methods are consistent within the framework of their uncertainties. The extrapolated cooperativity onset temperatures T_{on} for polystyrene and SBR 1500 are consistent with the crossover temperatures T_β from dielectric data, if the cooperativity is taken from the fluctuation approach to the glass transition based on von Laue thermodynamics.

Acknowledgements

We thank Drs. A. Heilmann and N. Teuscher (Frauenhofer Institut für Werkstoffmechanik Halle) for assistance with the infrared measurements, Drs. W. Seifert and K. Schröter (Universität Halle) for assistance with the corresponding computer simulation and discussions. Financial support by the Deutsche Forschungsgemeinschaft (SFB 418), the European Comission (IC15CT96-0821), and the Fonds Chemische Industrie (FCI) is acknowledged.

References

[1] S.H. Glarum, J. Chem. Phys. 33 (1960) 639.
[2] G. Adam, J.H. Gibbs, J. Chem. Phys. 43 (1965) 139.
[3] F. Mezei, W. Knaak, B. Farago, Phys. Rev. Lett. 58 (1987) 571.
[4] B. Frick, D. Richter, W. Petry, U. Buchenau, Z. Phys. B Condens. Matter 70 (1988) 73.
[5] W. Götze, L. Sjögren, Springer Conf. Proc. 20 (1988) 879.
[6] W. Laughlin, D. Uhlmann, J. Phys. Chem. 76 (1972) 2317.
[7] F. Stickel, E. Fischer, R. Richert, J. Chem. Phys. 102 (1995) 6251.
[8] G.P. Johari, M. Goldstein, J. Phys. Chem. 74 (1970) 2034.
[9] E. Rössler, Phys. Rev. Lett. 65 (1990) 1595.
[10] F. Fujara, B. Geil, H. Sillescu, G. Fleischer, Z. Phys. B Condensed Matter 88 (1992) 195.
[11] C. Donati, J.F. Douglas, W. Kob, S.J. Plimpton, P.H. Poole, S.C. Glotzer, Phys. Rev. Lett. 80 (1998) 2338.
[12] U. Tracht, M. Wilhelm, A. Heuer, H. Feng, K. Schmidt-Rohr, H. Spiess, Phys. Rev. Lett. 81 (1998) 2727.
[13] S. Reinsberg, X. Qui, M. Wilhelm, H. Spiess, M. Ediger, preprint.
[14] M. Arndt, R. Stannarius, H. Groothues, E. Hempel, F. Kremer, Phys. Rev. Lett. 79 (1997) 2077.
[15] E. Donth, E. Hempel, C. Schick, J. Phys.: Condens. Matter 12 (2000) L281.
[16] E. Donth, J. Non-cryst. Solids 53 (1982) 325.
[17] E. Hempel, G. Hempel, A. Hensel, C. Schick, E. Donth, J. Phys. Chem. B 104 (2000) 2460.
[18] E. Donth, The Glass Transition: Relaxation Dynamics in Liquids and Disordered Materials, Springer, Berlin, 2001.
[19] N.O. Birge, S.R. Nagel, Phys. Rev. Lett. 54 (1985) 2674.
[20] T. Christensen, J. Phys. France C8 12 (1985) C8.
[21] D. Jung, T. Kwon, D. Bae, I. Moon, Y.H. Jeong, Meas. Sci. Technol. 3 (1992) 475.
[22] H. Gobrecht, K. Hamann, G. Willers, J. Phys. E 4 (1971) 21.
[23] M. Reading, TRIP 1 (1993) 248.
[24] Proceedings of the IV Special Issue ''Temperature Modulated Calorimetry'', Ed. C. Schick and G.W.H. Höhne.
[25] J. Korus, E. Hempel, M. Beiner, S. Kahle, E. Donth, Acta Polym. 48 (1997) 369.
[26] H. Huth, M. Beiner, E. Donth, Phys. Rev. B 61 (2000) 15092.
[27] M. Beiner, S. Kahle, E. Hempel, K. Schröter, E. Donth, Europhys. Lett. 44 (1998) 321.
[28] C. Hansen, F. Stickel, T. Berger, R. Richert, E. Fischer, J. Chem. Phys. 107 (1997) 1086.
[29] C. Angell, K. Ngai, G. McKenna, P. McMillan, S. Martin, J. Appl. Phys. 88 (2000) 3113.
[30] A.P. Sokolov, Endeavour 21 (1997) 109.
[31] M. Beiner, H. Huth, K. Schröter, J. Non-Cryst. Solids 279 (2001) 126.
[32] S. Weyer, A. Hensel, J. Korus, E. Donth, C. Schick, Thermochim. Acta 304/305 (1997) 251.
[33] J. Korus, M. Beiner, K. Busse, S. Kahle, R. Unger, E. Donth, Thermochim. Acta 304/305 (1997) 99.
[34] B. Wunderlich, Y. Jin, A. Boller, Thermochim. Acta 238 (1994) 277.
[35] J. Schawe, Thermochim. Acta 260 (1995) 1.
[36] S. Weyer, A. Hensel, C. Schick, Thermochim. Acta 304/305 (1997) 267.
[37] A. Hensel, C. Schick, J. Non-cryst. Solids 235/237 (1998) 510.
[38] S. Sarge, W. Hemminger, E. Gmelin, G. Höhne, H. Cammenga, W. Eysel, J. Thermal Anal. 49 (1997) 1125.
[39] A. Hensel, C. Schick, Thermochim. Acta 304/305 (1997) 229.
[40] C. Schick, U. Jonsson, T. Vassiliev, A. Minakov, J. Schawe, R. Scherrenberg, D. Lorinczy, Thermochim. Acta 347 (2000) 53.
[41] S. Weyer, M. Merzlyakov, C. Schick, Thermochim. Acta, this issue.
[42] P.K. Dixon, S.R. Nagel, Phys. Rev. Lett. 61 (1988) 341.
[43] N. Menon, J. Chem. Phys. 105 (1996) 5246.
[44] I. Moon, Y. Jeong, S. Kwun, Rev. Sci. Instrum. 67 (1996) 29.
[45] I.K. Moon, K.-B. Jung, Lee, Y.H. Jeong, Appl. Phys. Lett. 76 (2000) 2451.

[46] U.G. Jonsson, O. Andersson, A. Fransson, Thermochim. Acta 347 (2000) 45.
[47] P. Kamasa, M. Merzlyakov, M. Pyda, J. Pak, C. Schick, B. Wunderlich, Thermochim. Acta, accepted.
[48] M. Merzlyakov, C. Schick, Thermochim. Acta 330 (1999) 55, 65.
[49] M. Merzlyakov, C. Schick, this issue.
[50] U.G. Jonsson, O. Andersson, Meas. Sci. Technol. 9 (1998) 1873.
[51] S. Matsuoka, Relaxation Phenomena in Polymers, Hanser, München, 1992 (Chapter 2).
[52] O. Yamamuro, I. Tsukushi, A. Lindqvist, S. Takahara, M. Ishikawa, T. Matsuo, J. Phys. Chem. B 102 (1998) 1605.
[53] G. Johari, J. Chem. Phys. 112 (2000) 8958.
[54] H. Sillescu, J. Non-cryst. Solids 243 (1999) 81.
[55] C. Moynihan, J. Schroeder, J. Non-cryst. Solids 160 (1993) 52.
[56] H. Sillescu, Acta Polymer. 45 (1994) 2.
[57] M. von Laue, Phys. Z 18 (1917) 542.
[58] E. Donth, J. Phys.: Condens. Matter 12 (2000) 10371.
[59] M. Beiner, S. Kahle, S. Abens, E. Hempel, S. Höring, M. Meissner, E. Donth, Macromolecules, submitted for publication.
[60] J. Brandup, E. Immergut, Polymer Handbook, 3rd Edition, Wiley, New York, 1989 (Chapter 5).
[61] N. Shito, J. Polym. Sci. C 23 (1968) 569.
[62] U. Pschorn, E. Rössler, H. Sillescu, S. Kaufmann, D. Schaefer, H. Spiess, Macromolecules 24 (1991) 398.
[63] K.-H. Illers, Z. Electrochem. 65 (1961) 679.